Acta Mech 229, 629–644 (2018)
https://doi.org/10.1007/s00707-017-1989-y

ORIGINAL PAPER

Friedrich Pfeiffer

On the structure of frictional impacts

This paper is dedicated to the memory of Franz Ziegler

Received: 20 February 2017 / Published online: 23 November 2017

Abstract Many processes in machines and mechanisms are accompanied by impacts with friction. They arise by short-time contacts between two or more bodies, and they generate energy losses mainly due to friction in tangential contact directions. During the last three decades, a couple of impact models based on the theory of rigid body contacts were established connected with the names of Moreau, Fremond, and Glocker, which all work quite satisfactorily with respect to practical applications. In the following, we shall establish the basic equations, discuss several structural issues, and consider the energy behavior of impulsive motion. Measurements verify the theoretical ideas very nicely. An application will be given, too.

1 Introduction

Impacts are contact processes of very short duration time, which generate in a small zone of the contact some typical deformations. Two arbitrarily approaching bodies with normal and tangential relative velocities produce normal and tangential impact forces, which deform the two bodies in normal and tangential directions and which include friction, though mainly in tangential direction. These deformations are accompanied by a partial conversion of the incoming kinetic energy into potential energy of the deformations, which act as a kind of spring on the bodies when moving apart again. The process generates energy losses by friction.

Modeling such processes requires the knowledge of the local stiffness around the point of contact. The corresponding forces put into the equations of motion usually lead to stiff differential equations. Such models make sense for problems, where we need to know the details of the impact deformations. For mechanical systems with many contacts, the method results in very large computing times due to the elastic resolution of the individual impacts.

An alternative approach consists in rigid body models. We go from the above force/acceleration level of the equations of motion to an impulse/velocity level by integrating the equations of motion during the very small assumed impact time. Or better, we use the concept of measure differential equations instead of the classical equations of motion as suggested by Moreau. Working on an impulse–velocity level instead on a force–acceleration level turns out to be sufficient for a large variety of engineering problems, especially for large systems with many unilateral contacts. We shall use also here the concepts of compression and expansion, which is clear for real local deformations, being built up during compression and released during expansion. For rigid contact models, it makes sense in a virtual way and for the definition of relative contact kinematics.

The topic belongs to the more general field of non-smooth mechanics, which originally has been founded by Moreau [11], Montpellier, who not only established the mechanical but also the mathematical basis of

F. Pfeiffer (✉)
Institute for Applied Mechanics, Technical University of Munich, Boltzmannstrasse 15, 85747 Garching, Germany
E-mail: friedrich.pfeiffer@tum.de
Tel.: +49-89-28915200
Fax: +49-89-28915213

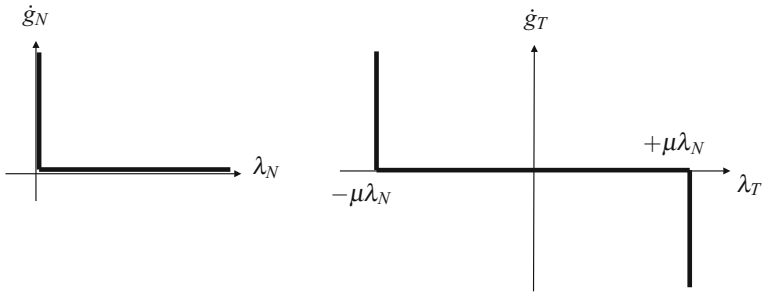

Fig. 1 Contact laws for impacts, left normal, right tangential direction

this new science, which represents a substantial extension of classical mechanics. As a matter of fact, it is more than an extension; classical mechanics is in a sense a subset of non-smooth mechanics. Panagiotopoulos [12], Thessaloniki, Greece, completed the new theories by introducing inequalities with regard to non-convex features. Moreau and Panagiotopoulos both apply the idea of complementarity as one important and basic element for the theory. Most of their applications refer to problems of elastomechanics. Nevertheless and from the very beginning, it was evident that the methods from Moreau and Panagiotopoulos could also be transferred to multibody dynamics [14–16].

A very modern and comprehensive presentation of the problems connected with frictional impacts is given by the papers [8,9] confirming also the progress made during the last years on the mathematical side but also with respect to a deeper insight into the mechanical problems.

2 Models

2.1 Classical approaches

With concern to classical theory, we refer to [14,16]. For contacts, we have the equations of motion together with the relative acceleration within the contact (N normal, T tangential, R sliding friction)

$$\begin{aligned} &M\ddot{q} - h - (W_N + H_R \quad W_T)\begin{pmatrix}\lambda_N\\ \lambda_T\end{pmatrix} = 0 \quad \in \mathbb{R}^f,\\ &\ddot{g}_N = W_N^T\ddot{q} + \overline{w}_N \quad \in \mathbb{R}^{n_N},\\ &\ddot{g}_T = W_T^T\ddot{q} + \overline{w}_T \quad \in \mathbb{R}^{n_T} \end{aligned} \tag{1}$$

where relative kinematics is put on an acceleration level. Originally, they are on a position/orientation and on a velocity level. In addition, we have the complementarity conditions in normal and tangential directions. In normal direction, we get, see Fig. 1 left,

$$\dot{g}_N \geq 0, \quad \lambda_N \geq 0, \qquad \dot{g}_N^T\lambda_N = 0. \tag{2}$$

The conditions in tangential direction are (Fig. 1 right)

$$\begin{aligned} &|\lambda_{Ti}| < \mu_{0i}\lambda_{Ni} \quad \wedge\ \dot{g}_{Ti} = 0 \quad (i \in I_T \ \text{sticking}),\\ &\lambda_{Ti} = +\mu_{0i}\lambda_{Ni} \quad \wedge\ \dot{g}_{Ti} \leq 0 \quad (i \in I_N \backslash I_T \ \text{ neg. sliding}),\\ &\lambda_{Ti} = -\mu_{0i}\lambda_{Ni} \quad \wedge\ \dot{g}_{Ti} \leq 0 \quad (i \in I_N \backslash I_T \ \text{ pos. sliding}) \end{aligned} \tag{3}$$

which also can be written in the form

$$y = Ax + b, \qquad y \geq 0, \quad x \geq 0, \quad y^T x = 0, \quad y, x \in \mathbb{R}^{n^*} \tag{4}$$

where $n^* = n_N + 4n_T$ in the case of decomposition into four and $n^* = n_N + 2n_T$ for a decomposition into two elementary corners, called "unilateral primitives" [7]. The quantities are: M mass matrix, q vector of generalized coordinates including the bilateral constraints, $W_{N,T}$ the constraint matrices due to contacts, H

the sliding friction matrix, $\lambda_{N,T}$ the constraint forces, $(\dot{g}_{N,T},\ \ddot{g}_{N,T})$ relative velocities and accelerations in the contact, μ_{0i} friction coefficients in Coulomb's law, and the following index sets:

$$\begin{aligned} I_A &= \{1, 2, \ldots, n_A\} && \text{with } n_A \text{ elements,} \\ I_C(t) &= \{i \in I_A : g_{Ni} = 0\} && \text{with } n_C \text{ elements,} \\ I_N(t) &= \{i \in I_C(t) : \dot{g}_{Ni} = 0\} && \text{with } n_N \text{ elements,} \\ I_T(t) &= \{i \in I_N(t) : |\dot{g}_{Ti}| = 0\} && \text{with } n_T \text{ elements.} \end{aligned} \tag{5}$$

Considering impacts with friction, we have to put these equations on a velocity level by integration over the impact time, which is as usual assumed to be infinitesimally short [6,16]. Denoting the beginning of an impact, the end of compression and the end of expansion by the indices A, C, E, respectively, we get for $\Delta t = t_E - t_A$

$$\begin{aligned} &M(\dot{q}_C - \dot{q}_A) - (W_N \ \ W_T) \begin{pmatrix} \Lambda_{NC} \\ \Lambda_{TC} \end{pmatrix} = 0, \\ &M(\dot{q}_E - \dot{q}_C) - (W_N \ \ W_T) \begin{pmatrix} \Lambda_{NE} \\ \Lambda_{TE} \end{pmatrix} = 0 \qquad \text{with} \quad \Lambda_i = \lim_{t_E \to t_A} \int_{t_A}^{t_E} \lambda_i \mathrm{d}t. \end{aligned} \tag{6}$$

Here Λ_{NC}, Λ_{TC} are the impulses in the normal and tangential direction which are transferred during compression, and Λ_{NE}, Λ_{TE} those of expansion. Defining $\dot{q}_A = \dot{q}(t_A)$, $\dot{q}_C = \dot{q}(t_C)$, $\dot{q}_E = \dot{q}(t_E)$ we express the relative velocities by [16]

$$\begin{aligned} \begin{pmatrix} \dot{g}_{NA} \\ \dot{g}_{TA} \end{pmatrix} &= \begin{pmatrix} W_N^T \\ W_T^T \end{pmatrix} \dot{q}_A + \begin{pmatrix} \tilde{w}_N \\ \tilde{w}_T \end{pmatrix}, \\ \begin{pmatrix} \dot{g}_{NE} \\ \dot{g}_{TE} \end{pmatrix} &= \begin{pmatrix} W_N^T \\ W_T^T \end{pmatrix} \dot{q}_E + \begin{pmatrix} \tilde{w}_N \\ \tilde{w}_T \end{pmatrix}, \\ \begin{pmatrix} \dot{g}_{NC} \\ \dot{g}_{TC} \end{pmatrix} &= \begin{pmatrix} W_N^T \\ W_T^T \end{pmatrix} \dot{q}_C + \begin{pmatrix} \tilde{w}_N \\ \tilde{w}_T \end{pmatrix}. \end{aligned} \tag{7}$$

The matrices W are the constraint Jacobians, which project the motion into the possible free directions. The vectors $\tilde{w}$ result from external excitations, whatsoever.

Considering in a first step the compression phase and combining the Eqs. (6) and (7) we come out with

$$\begin{pmatrix} \dot{g}_{NC} \\ \dot{g}_{TC} \end{pmatrix} = \underbrace{\begin{pmatrix} W_N^T \\ W_T^T \end{pmatrix} M^{-1} \begin{pmatrix} W_N \\ W_T \end{pmatrix}^T}_{G} \cdot \begin{pmatrix} \Lambda_{NC} \\ \Lambda_{TC} \end{pmatrix} + \begin{pmatrix} \dot{g}_{NA} \\ \dot{g}_{TA} \end{pmatrix} \tag{8}$$

where G is called the matrix of projected inertia. It consists of four blocks G_{NN}, G_{NT}, G_{TN}, G_{TT}. The mass projection matrix G is quadratic and symmetric, for the case with dependent constraints positive semi-definite, otherwise positive definite. The submatrices G_{NN}, G_{TT} possess the same properties as G and $G_{NT} = G_{TN}^T$ [3]. Equation (8) permits calculation of the relative velocities $\dot{g}_{NC}$ and $\dot{g}_{TC}$ at the end of the compression phase, depending on the velocities at the beginning of the impact $\dot{g}_{NA}$ and $\dot{g}_{TA}$ under the influence of the contact impulses Λ_{NC} and Λ_{TC}.

To evaluate these impulses two impact laws in normal and tangential direction are necessary. As already indicated magnitudes of relative kinematics and constraint forces (here impulses) are complementary quantities. In normal direction these are $\dot{g}_{NC}$ and Λ_{NC}. In tangential direction we have the relative tangential velocity vector $\dot{g}_{TC}$ and the friction surplus $\Lambda_{TC} - (\mathrm{diag}\mu_{0i})\Lambda_{NC}$, which is the distance of the relevant constraint impulse Λ_{TC} to the friction cone boundary for the contact under consideration. Decomposing the tangential behavior we obtain:

$$\begin{aligned} \Lambda_{TCV,i} &= \Lambda_{TC,i} + \mu_i \Lambda_{TN,i}, \\ \dot{g}_{TC,i} &= \dot{g}_{TC,i}^{+} - \dot{g}_{TC,i}^{-}, \\ \Lambda_{TCV,i}^{(+)} &= \Lambda_{TCV,i}, \\ \Lambda_{TCV,i}^{(-)} &= -\Lambda_{TCV,i} + 2\mu_i \Lambda_{NC,i}. \end{aligned} \tag{9}$$

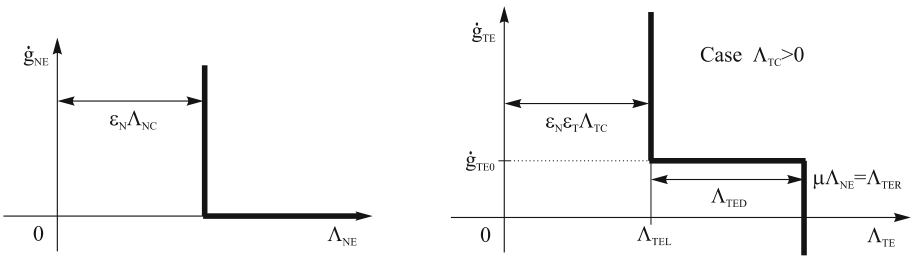

Fig. 2 Shifted normal and tangential characteristics for impact expansion

Together with Eq. (8) this results in a Linear Complementary Problem (LCP) in standard form $y = Ax + b$ with $x \geq 0,\ \ y \geq 0$ and $x^T y = 0$:

$$\underbrace{\begin{pmatrix} \dot{g}_{NC} \\ \dot{g}_{TC}^{+} \\ \Lambda_{TCV}^{(-)} \end{pmatrix}}_{y} = \underbrace{\begin{pmatrix} G_{NN} - G_{NT}\mu & G_{NT} & 0 \\ G_{TN} - G_{TT}\mu & G_{TT} & E \\ 2\mu & -E & 0 \end{pmatrix}}_{A} \underbrace{\begin{pmatrix} \Lambda_{NC} \\ \Lambda_{TCV}^{(+)} \\ \dot{g}_{TC}^{-} \end{pmatrix}}_{x} + \underbrace{\begin{pmatrix} \dot{g}_{NA} \\ \dot{g}_{TA} \\ 0 \end{pmatrix}}_{b}. \tag{10}$$

μ is a diagonal matrix, containing the friction coefficients of the contacts. The problem has to be solved numerically. The velocities $\dot{g}_{NC},\ \dot{g}_{TC}$ and the impulses $\Lambda_{NC},\ \Lambda_{TC}$ are either part of the result or can be obtained by the transformation (9) and by $\Lambda_{TC} = \Lambda_{TCV}^{(+)} - \mu\Lambda_{NC}$.

In the compression phase, the kinetic energy of the colliding bodies is stored as potential energy. During the expansion phase, parts of this energy are released. This regaining process is governed by two coefficients of restitution in normal and tangential directions ε_N and ε_T, respectively. They are empirical coefficients and must be measured.

In the case of multiple impacts, Poisson's friction law does not guarantee impenetrability of the bodies. So the law is enhanced by an additional condition. The normal impulse during the phase of restitution Λ_{NE} is minimum with $\varepsilon_E\Lambda_{NC}$ in each contact, but can become arbitrarily large to avoid penetration. In this case, the bodies remain in contact after the impact. This impact law with its complementary character is drawn in Fig. 2.

In tangential direction the impact law is ruled by the following effects: at first a minimum impulse $[\varepsilon_N(\varepsilon_T\Lambda_{TC})]$ must be transferred. It is the impulse stored during compression reduced by losses due to Poisson's law, but as all contact actions in tangential direction are always connected with constraints in normal direction we have to consider also a loss due to ε_N. In addition, the impulse must not exceed the friction limits. Between these limits a tangential relative velocity $\dot{g}_{TE0}$ appears, which is generated by an elastic effect: For tangential contacts, we get an elastic compression of the local contact zone, which acts as a spring. The point of application of this tangential spring force is different from the contact point thus giving rise to a possible local tangential velocity. This velocity allows a restitution of the stored energy if during the phase of restitution sticking occurs. The existence of $\dot{g}_{TE0}$ was detected by Beitelschmidt's measurements [3], and it could be derived as a necessary correction. With

$$\dot{g}_{TE0} = G_{TN}\varepsilon_N\Lambda_{NC} + G_{TT}\varepsilon_N\varepsilon_T\Lambda_{TC}, \tag{11}$$

one can calculate $\dot{g}_{TE0}$ for all contacts, and the tangential impact law looks like drawn in Fig. 2. ε_N and ε_T are diagonal matrices containing the different coefficients for all contacts. To formulate the equation for the phase of restitution as a LCP similar to the compression phase, the two matrices

$$\begin{aligned} S^{+} &= \operatorname{diag}\left(\tfrac{1}{2}\left(1 + \operatorname{sign}(\Lambda_{TC,i})\right)\right), \\ S^{-} &= \operatorname{diag}\left(\tfrac{1}{2}\left(1 - \operatorname{sign}(\Lambda_{TC,i})\right)\right) \end{aligned} \tag{12}$$

are helpful. After some transformations similar to those of the compression phase, the LCP writes (Eq. 4, $y = Ax + b$)

$$\begin{pmatrix} \dot{g}_{NE} \\ \dot{g}_{TEV}^{+} \\ \Lambda_{TEV}^{(-)} \end{pmatrix} = \begin{pmatrix} G_{NN} - G_{NT}S^{-}\mu & G_{NT} & 0 \\ G_{TN} - G_{TT}S^{-}\mu & G_{TT} & E \\ \mu & -E & 0 \end{pmatrix} \begin{pmatrix} \Lambda_{NP} \\ \Lambda_{TEV}^{(+)} \\ \dot{g}_{TEV}^{-} \end{pmatrix} + b \tag{13}$$

with

$$b = \begin{pmatrix} G_{NN}\varepsilon_N\Lambda_{NC} + G_{NT}S^+\varepsilon_N\varepsilon_T\Lambda_{TC} - G_{NT}S^-\mu\varepsilon_N\Lambda_{NC} + \dot{g}_{NC} \\ G_{TT}(S^+ - E)\varepsilon_N\varepsilon_T\Lambda_{TC} - G_{TT}S^-\mu\varepsilon_N\Lambda_{NC} + \dot{g}_{TC} \\ \mu\varepsilon_N\Lambda_{NC} - \varepsilon_N\varepsilon_T|\Lambda_{TC}| \end{pmatrix}. \tag{14}$$

After a corresponding solution the velocities $\dot{g}_{NC}, \dot{g}_{TC}$ and the impulses $\Lambda_{NC}, \Lambda_{TC}$ are either part of the result or can be obtained by the transformations:

$$\dot{g}_{TE} = \dot{g}^+_{TEV} - \dot{g}^-_{TEV} + \dot{g}_{TE0}, \tag{15}$$

$$\Lambda_{NE} = \Lambda_{NP} + \varepsilon_N\Lambda_{NC},$$

$$\Lambda_{TE} = \Lambda^{(+)}_{TEV} + \Lambda_{TEL} = \Lambda^{(+)}_{TEV} + S^+\varepsilon_N\varepsilon_T\Lambda_{TC} - S^-\mu\Lambda_{NE}. \tag{16}$$

If the impulses during the two phases of the impact are known, one can calculate the motion $\dot{q}_E$ of the multibody system at the end of the impact,

$$\dot{q}_E = \dot{q}_A M^{-1}\left(W_N(\Lambda_{NC} + \Lambda_{NE}) + W_T(\Lambda_{TC} + \Lambda_{TE})\right). \tag{17}$$

2.2 Recent approaches

Moreau [11] suggested measure differential equations representing the equations of motion for systems with non-continuous phenomena. These equations contain a Lebesgue-measurable part for the continuous components and an atomic part based on a Dirac point measure for the impact parts (see also [7]). They read with $u = \dot{q}$

$$M(q,t)\mathrm{d}u - h(u,q,t)\mathrm{d}t - W_N(q,t)\mathrm{d}\Lambda_N - W(q,t)\mathrm{d}\Lambda_T = 0. \tag{18}$$

The measure for the velocities $\mathrm{d}u = \dot{u}\mathrm{d}t + (u^+ - u^-)\mathrm{d}\eta$ is split in a Lebesgue-measurable part $\dot{u}\mathrm{d}t$, which is continuous, and the atomic parts which occur at the discontinuity points with the left and right limits u^+ and u^- and the Dirac point measure $\mathrm{d}\eta$. Similarly, the measure for the impulses is defined as $\mathrm{d}\Lambda = \lambda\mathrm{d}t + \Lambda\mathrm{d}\eta$.

In addition to this more general approach for the equations of motion we introduce a novel concept for the inequality constraints which originally comes from the linear programming field. It applies the proximal point idea from convex analysis [17] to develop the so-called "Augmented Lagrange Method" [1]. The proximal point of a convex set C to a point z is the closest point in C to z [10],

$$\mathrm{prox}_C(z) = \arg\min_{x^*\in C}|z - x^*|, \quad z \in \mathbb{R}^n, \tag{19}$$

which is illustrated in Fig. 3. If we understand this convex set as the cut of a friction cone with different friction coefficients in the two contact directions, then every solution of the system falling outside the convex set is brought back to the boundary of the set. In the case of a complementarity in normal direction (contact/detachment case), the set is just the half space with nonnegative constraint forces λ_N. Therefore, we get the relations

$$\lambda_N = \mathrm{prox}_{C_N}(\lambda_N - r g_N) \tag{20}$$

where C_N denotes the set of admissible normal contact forces,

$$C_N(\lambda_N) = \{\lambda_N | \lambda_N \geq 0\}. \tag{21}$$

In the same manner we can put Coulomb's friction law (3) into the form

$$\lambda_T = \mathrm{prox}_{C_T(\lambda_N)}(\lambda_T - r\dot{g}_T) \tag{22}$$

with C_T denoting the set of admissible tangential forces,

$$C_T(\lambda_N) = \{\lambda_T | \quad |\lambda_{Ti}| \leq \mu_{0i}\lambda_{Ni}\}. \tag{23}$$

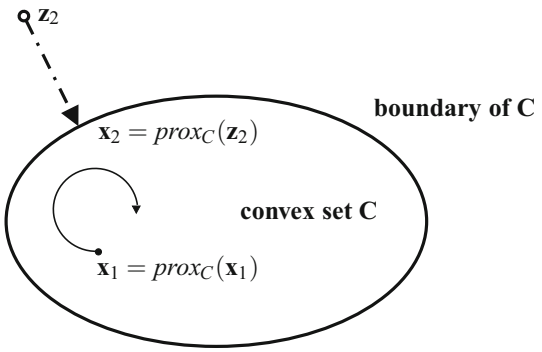

Fig. 3 The proximal point in convex analysis

At this point we have to discuss the above expressions in more detail. We follow partly the very clear description of convex properties in the book of Leine [10]. He interprets the basic relationship for the constraints ($\lambda = \text{prox}_C(\lambda - rg)$) as an "exact regularization," where r is the steepness parameter of this regularization. The above expression replaces the non-smooth contact laws by a prox-function, which is usually nonlinear, but which allows at the same time to reduce the whole system of the equations of motion together with the inequality constraints to a point mapping set. It can be treated by modern and well-known numerical methods.

Coming back to the expression ($\lambda = \text{prox}_C(\lambda - rg)$) we see by a more heuristic consideration the following features: The relation can be satisfied only by left-hand and right-hand side expressions of equal sign or by left-hand and right-hand side expressions, which are zero. From this we may conclude the following results for a holonomic case (see [4,5])

$$(\lambda = \text{prox}_C(\lambda - rg)) \ \wedge \ (r > 0) \ \sim \ \begin{cases} \lambda = \lambda - rg & \text{if} \ \ \lambda - rg \geq 0 \\ \lambda = 0 & \text{if} \ \ \lambda - rg < 0. \end{cases} \tag{24}$$

The first case corresponds to an active contact with contact and no detachment, or it corresponds for the case ($g \ \rightarrow \ \dot{g}$) to an active tangential contact with stiction. The second case corresponds to a passive contact state. A more thorough consideration with respect to the equivalence of complementarities and the prox-representation may be found in [1,10]. An excellent work with respect to this equivalence is given by [19].

Combining the contact laws (20) and (22) together with the equations of motion (18), we obtain a set of non-smooth continuous equations for the unknowns $\ddot{q}$, λ_N and λ_T,

$$\begin{aligned} M(q,t)\mathrm{d}u - h(u,q,t)\mathrm{d}t - W_N(q,t)\mathrm{d}\Lambda_N - W(q,t)\mathrm{d}\Lambda_T &= 0, \\ \lambda_N - \text{prox}_{C_N}(\lambda_N - r\ddot{g}_N) &= 0, \\ \lambda_T - \text{prox}_{C_T(\lambda_N)}(\lambda_T - r\ddot{g}_T) &= 0, \end{aligned} \tag{25}$$

which is a convenient form for applying the time stepping algorithm together with the Augmented Lagrange Idea for a numerical solution. It should be noted that the above equations contain the mechanics of general contacts and also the dynamics of impacts with friction.

3 Energy losses

The loss of energy is the difference of the total system energy after an impact and before an impact. In terms of the generalized velocities $\dot{\mathbf{q}}$ we write

$$\begin{aligned} \Delta T &= T_E - T_A \quad \leq \quad 0, \\ \Delta T &= \frac{1}{2}\dot{q}_E^T M \dot{q}_E - \frac{1}{2}\dot{q}_A^T M \dot{q}_A = \frac{1}{2}(\dot{q}_E + \dot{q}_A)^T M (\dot{q}_E - \dot{q}_A). \end{aligned} \tag{26}$$

These are expressions considering scleronomic systems without an excitation by external kinematic sources. Applying the relations as presented in [16], we get for the energy expression the form

$$2\Delta T = 2\Delta T_1 + \Delta T_2 = +2\begin{pmatrix}\dot g_{NE}\\ \dot g_{TE}\end{pmatrix}^T\left[\begin{pmatrix}\mathbf{\Lambda}_{NC}\\ \mathbf{\Lambda}_{TC}\end{pmatrix}+\begin{pmatrix}\mathbf{\Lambda}_{NE}\\ \mathbf{\Lambda}_{TE}\end{pmatrix}\right]- \\ -\left[\begin{pmatrix}\mathbf{\Lambda}_{NC}\\ \mathbf{\Lambda}_{TC}\end{pmatrix}+\begin{pmatrix}\mathbf{\Lambda}_{NE}\\ \mathbf{\Lambda}_{TE}\end{pmatrix}\right]^T G\left[\begin{pmatrix}\mathbf{\Lambda}_{NC}\\ \mathbf{\Lambda}_{TC}\end{pmatrix}+\begin{pmatrix}\mathbf{\Lambda}_{NE}\\ \mathbf{\Lambda}_{TE}\end{pmatrix}\right]$$

$$\text{with}\qquad G=\begin{pmatrix}G_{NN}\ G_{NT}\\ G_{TN}\ G_{TT}\end{pmatrix}\quad\text{where}\quad G_{ij}=W_i^T M^{-1}W_j,\quad i,j\in\{N,T\}. \tag{27}$$

G is the mass projection matrix, which is quadratic and positive definite with the exception of dependent constraints, where it is semi-definite. The $\dot g$ are relative contact velocities and the $\mathbf{\Lambda}$ impulses. The indices N, T stand for normal and tangential, respectively, and the indices C, E for the end of compression and the end of expansion, respectively. The second term of the energy equation is a quadratic form and for itself always positive or zero, and from this we have $\Delta T_2 \le 0$, always. The energy loss has to be negative, which will be decided by the first term of the above relations. If this term is negative or at least zero, the condition $\Delta T \le 0$ will hold. Therefore, we shall concentrate on the first term which reads in more detail

$$2\Delta T_1 = +2\begin{pmatrix}\dot g_{NE}\\ \dot g_{TE}\end{pmatrix}^T\left[\begin{pmatrix}\mathbf{\Lambda}_{NC}\\ \mathbf{\Lambda}_{TC}\end{pmatrix}+\begin{pmatrix}\mathbf{\Lambda}_{NE}\\ \mathbf{\Lambda}_{TE}\end{pmatrix}\right]=2\left[\dot g_{NE}^T(\mathbf{\Lambda}_{NC}+\mathbf{\Lambda}_{NE})+\dot g_{TE}^T(\mathbf{\Lambda}_{TC}+\mathbf{\Lambda}_{TE})\right]. \tag{28}$$

For the evaluation of this equation, we have to discuss the models. The compression/expansion model as considered here is a very powerful one and approved by many applications providing us with the necessary information for impulsive processes in multibody systems, but it does not provide us with the details within the compression and expansion phases necessary for energy considerations. We get an information at three points A, C, E (A = beginning, C = end compression, E = end expansion), but not between these points.

We know, for example, that for an impact with sliding or sticking the relative normal distance and velocity have to be zero. Otherwise, we do not get tangential impact and contact motion. But, on the other hand, the results for the points A, C, E would give us for E only a nonzero normal velocity, which appears in physical reality only at the very end of the impact and not during expansion. To solve this problem without ruining the model concept, it is sufficient to define the transition locations at the very end of the compression phase [transition (C/E)] and of the expansion phase (point E). Such transitions from sticking to sliding or vice versa and from contact to detachment are assumed to take place in an infinitesimally short time with no energy effects.

So it can be shown that the first term $\dot g_{NE}^T(\mathbf{\Lambda}_{NC}+\mathbf{\Lambda}_{NE})$ of the energy Eq. (28) is not zero due to positive normal impulses $(\mathbf{\Lambda}_{NC}+\mathbf{\Lambda}_{NE})$ and due to a nonzero end velocity $\dot g_{NE}$ after the impact, which is physically reasonable for a separation of the two contacting bodies. But, on the other hand, sliding or sticking during expansion requires a zero normal relative velocity $\dot g_{NE}$ in the contact, which makes the above mentioned term to zero. The $\mathbf{\Lambda}_{NE}$-value slips into the corner of Fig. 2 allowing the system to build up the necessary separation velocity. From this we assume that during the expansion phase the term $\dot g_{NE}^T(\mathbf{\Lambda}_{NC}+\mathbf{\Lambda}_{NE})=0$ is zero.

As a result of these arguments and of the last condition of continuous contact during the impact, we get for compression and expansion $\mathbf{\Lambda}_N > 0$ and $\dot g_N = 0$, which is also part of the complementarity, and therefore simply

$$2\Delta T_1 = 2\dot g_{TE}^T(\mathbf{\Lambda}_{TC}+\mathbf{\Lambda}_{TE}), \tag{29}$$

the sign of which has to be investigated. For this purpose, we consider this equation with respect to the following four cases; see for the arguments always Figs. 1 and 2:

– *sticking during compression, sticking during expansion*

The tangential impulses have to be within the appropriate friction cones. The tangential velocities are zero, and therefore, we need not to consider the magnitudes of the impulses,

$$-\mathrm{diag}(\mu_0)\mathbf{\Lambda}_{NC} \le \mathbf{\Lambda}_{TC} \le +\mathrm{diag}(\mu_0)\mathbf{\Lambda}_{NC},\quad \mathbf{\Lambda}_{TEL} \le \mathbf{\Lambda}_{TE} \le \mathbf{\Lambda}_{TER}$$
$$\Longrightarrow\quad \dot g_{TE}^T(\mathbf{\Lambda}_{TC}+\mathbf{\Lambda}_{TE})=0.$$

– *sliding during compression, sliding during expansion*

Sliding means single-valued impulse laws according to Coulomb's law. Some difficulties will appear for the cases with reversed sliding, that means, with a tangential relative velocity the sign of which is different during compression and during expansion. Therefore, we have to consider the two cases without and with tangential reversibility. For the first case, we do not have a change of sign of the relative tangential velocity, which gives $\text{sign}(\dot{g}_{TC}) = \text{sign}(\dot{g}_{TE})$. This comes out with the relations:
$\dot{g}_{TE}^T \mathbf{\Lambda}_{TC} = -\dot{g}_{TE}^T[\text{diag}(\mu)\text{sign}(\dot{g}_{TE})\mathbf{\Lambda}_{NC}] = -\text{diag}(\mu)|\dot{g}_{TE}|\mathbf{\Lambda}_{NC} \leq \mathbf{0}$,
$\Longrightarrow \quad \dot{g}_{TE}^T(\mathbf{\Lambda}_{TC} + \mathbf{\Lambda}_{TE}) < 0.$
The case with tangential reversibility is more complicated, because it includes a change of sign of the tangential relative velocity and thus at least an extremely short stiction phase, which we put exactly at the point (end of compression)/(beginning of expansion). The sliding velocity during compression decreases until it arrives at one of the corners of Fig. 1, then we get an extremely short shift from this corner to the other one, which allows the contact to build up a tangential velocity with an opposite sign, then valid for the expansion phase. Only by such a short stiction phase a reversal of tangential velocity is possible. On the other hand, such a transition from stick to slip, as short as it might be, follows the same process as for the next case sticking/sliding. Therefore, it is dissipative:
$\Longrightarrow \quad \dot{g}_{TE}^T(\mathbf{\Lambda}_{TC} + \mathbf{\Lambda}_{TE}) < 0.$

– *sticking during compression, sliding during expansion*

The transition from sticking in compression and sliding in expansion follows the mechanism (Fig. 1): If $\mathbf{\Lambda}_{TC} \gtrless \mathbf{0}$, then sliding is only possible for being at the very end of compression on the friction cone boundary with $\mathbf{\Lambda}_{TC} = \pm\text{diag}(\mu)\mathbf{\Lambda}_{NC}$ and $\dot{g}_{TC-at} \lessgtr \mathbf{0}$ (at = after transition stick-slip). This results always in a negative sign of the expression $(\dot{g}_{TE}^T\mathbf{\Lambda}_{TC})$. For the rest we assume a continuation of the signs after going from stick to slip $[\text{sign}(\dot{g}_{TE}) = \text{sign}(\dot{g}_{TC-at})]$. Then we arrive at:
$\Longrightarrow \quad \dot{g}_{TE}^T(\mathbf{\Lambda}_{TC} + \mathbf{\Lambda}_{TE}) < 0.$

– *sliding during compression, sticking during expansion*

This case is again simpler, because we get sticking at the end with a zero relative tangential velocity. Therefore we need not to consider the impulses.
$\Longrightarrow \quad \dot{g}_{TE}^T(\mathbf{\Lambda}_{TC} + \mathbf{\Lambda}_{TE}) = 0.$

– *summarized result for all cases*
$\Longrightarrow \quad \dot{g}_{TE}^T(\mathbf{\Lambda}_{TC} + \mathbf{\Lambda}_{TE}) \leq 0 \quad \Longrightarrow \quad \Delta T_1 \leq 0 \quad \Longrightarrow \quad \Delta T \leq 0.$

One may object that the above considerations assume in the case of multiple impacts the same impact structure for all simultaneously appearing impacts, which is usually not true. But even any combination of the above four cases for simultaneous impacts gives a loss of energy. Practical experience indicates in addition that the simultaneous appearance of impacts is extremely scarce, and it is an event, which nearly does not happen.

As a final result, we may state that the above evaluation confirms the physical argument, that any impact processes are accompanied by energy losses. This confirms also the well-known statement of Carnot (1803) [13], that "in the absence of impressed impulses, the sudden introduction of stationary and persistent constraints that change some velocity reduces the kinetic energy. Hence, by the collision of inelastic bodies, some kinetic energy is always lost".

The above considerations and the underlying theory have been confirmed not only by the experimental work of Beitelschmidt [3], but also by many industrial projects where the non-smooth methods were applied.

4 Experiments

With respect to large technical applications impacts with friction play such an important role, that a really applicable theory came amazingly late. The first ideas regarding large dynamical systems with frictional impacts are contained in the famous contribution of Moreau in the year 1988 [11], but then more or less applied to static or quasi-static (smaller) problems. During the 1990s, these ideas were included into multibody theory by [3,6,16] and applied to large industrial problems, which without exception confirmed the relevant theories. In addition a thorough and systematic experimental proof of the theory has been performed by Beitelschmidt [2,3].

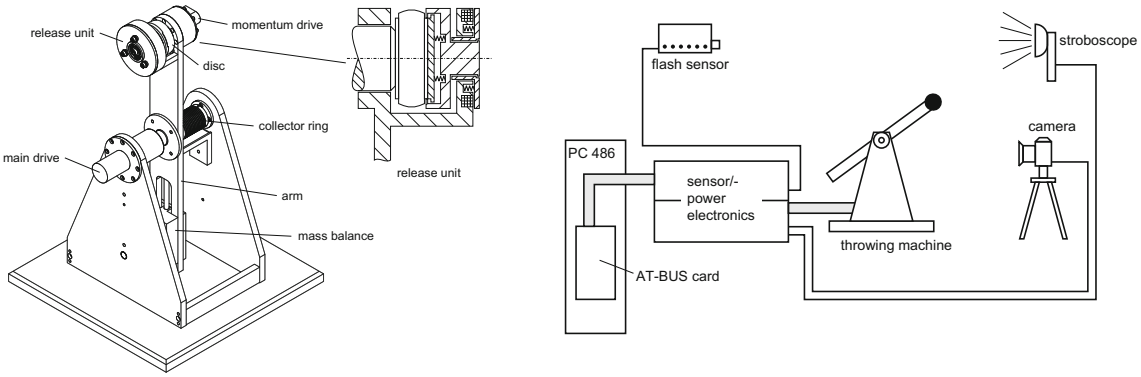

Fig. 4 Left principle of the throwing machine and right structure of the test setup

In the following, we shall focus on these experiments. In designing a test setup for measuring impacts with friction a first principal decision had to be made with respect to the experiments and to the geometrical type of impact, plane or spatial. Colliding bodies moving in a plane include linear complementarity problems, spatial contacts generate nonlinear complementarities. Therefore, motion in a plane was considered where one body is a disk and the other one the ground. On this basis, some further requirements had to be defined:

- maximum translational velocity 10 m/s
- maximum rotational velocity 40 rps
- throw direction $0° - 90°$
- release time < 12 ms
- encoder main axis 1600 points
- encoder momentum axis 400 points
- throwing disk diameter 50 mm, thickness 20 mm, weight 300 g
- continuous variable velocity control
- translation and rotation decoupled
- disturbance-free support and release of disk
- mass balance, statically and dynamically
- electric drives (pulse width modulation with 250 steps)
- automatic control for the throwing process, the release of stroboscope and camera

As a result, the machine shown in Fig. 4 was designed and realized, which meets all requirements. A release unit containing the disk is mounted at the end of a rotating arm with mass balance. The unit itself drives the disk giving it a prescribed rotational speed. The arm drive and momentum drive are decoupled allowing to control the two speeds independently. The rotation of the arm can be used to generate a translation, the rotation of the release unit realizes a rotation of the disk. Both mechanisms require an extremely precise time management of the release process. The flight of the body is photographed under stroboscopic exposure in a dark room before and after hitting its target. From the evaluation of the photographs, one can calculate the velocities and the position of the body immediately before and after the impact.

Figure 4 depicts the structure of the test setup. A computer performs all control calculations, processes sensor data, evaluates control torques, releases stroboscope and camera, and records all measured data. Within this overall structure, we find for each drive an individual control concept, which has thoroughly been optimized with regard to the above requirements [3]. Also, a typical sequence of events for the test procedure can be seen from Fig. 5. All computer codes have been realized in C++, which was feasible due to the fact that the PC mode activities are not critical with respect to time.

The evaluation of the measurements as recorded by the camera and the processor was straightforward. Figure 6 illustrates the method and depicts additionally a photograph of an experiment. The rubber disk experiment shows nicely a reversal of the trajectory due to the disk's rotation. The experimental process provided thus a very precise and well-reproducible basis for determining the properties of impacts with friction.

In the following, we shall give only a few examples out of more than 600 experiments performed with axisymmetric and with eccentric disks. In all cases the comparisons with theory come out with a good to

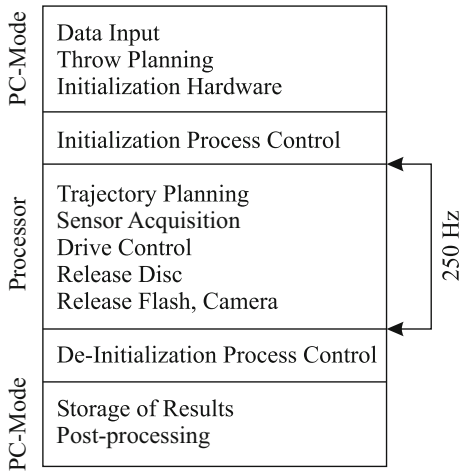

Fig. 5 Sequence of events of the throwing machine control

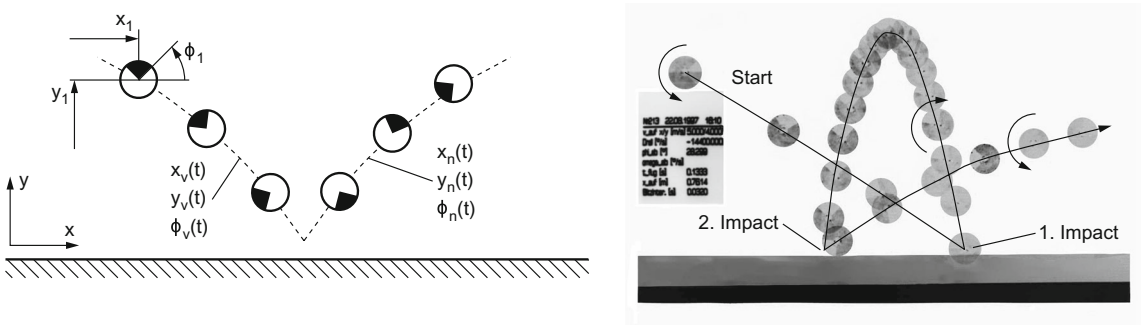

Fig. 6 Disk trajectory during an experiment, left method of evaluation, right photograph rubber

excellent correspondence [3]. In the subsequent diagrams, we shall use dimensionless velocities defined by

$$\gamma = \frac{\dot{g}_{TA}}{-\dot{g}_{NA}}, \qquad \gamma_{NC} = \frac{\dot{g}_{NC}}{-\dot{g}_{NA}}, \qquad \gamma_{TC} = \frac{\dot{g}_{TC}}{-\dot{g}_{NA}},$$
$$\gamma_{NE} = \frac{\dot{g}_{NE}}{-\dot{g}_{NA}}, \qquad \gamma_{TE} = \frac{\dot{g}_{TE}}{-\dot{g}_{NA}}, \qquad \gamma_{TE0} = \frac{\dot{g}_{TE0}}{-\dot{g}_{NA}} \tag{30}$$

where the indices N, T refer to normal and tangential directions. The indices A, C, E are the beginning and the end of the compression phase, and the end of the expansion phase, respectively. The kinematic magnitude $\dot{g}$ is a relative velocity in the contact zone. Experiments usually generate a negative normal velocity $(-\dot{g}_{NA})$ at the beginning.

Figure 6 also indicates the evaluation process for all experimental results. For every small part of the trajectory, we perform three stroboscope flashes thus achieving a certain redundancy for the measurements. The trajectory is approximately a parabola, and the velocity possesses a positive component in x- and a negative component in y-direction. The stroboscopic measurements in connection with the marked sectors of the disks allow a safe evaluation of the translational and rotational velocities of the disks. To find the time and the point of impact, the measurements before and after such an impact are represented by a statistical interpolation scheme, which allows to determine the impact together with the dispersion of the results.

The right part of Fig. 6 represents a spectacular case. The rubber disk appears from the left side with a horizontal velocity of 5 m/s and a vertical velocity of 4 m/s in negative y-direction. The rotational velocity in a counterclockwise direction amounts to 40 rps (2400 rpm). This results in a tangential relative velocity of 12.5 m/s at the point of impact. After the first contact, the velocities reverse by the impact jump, and the disk flies backward with a clockwise rotation. At the second impact the velocities change again, and the disk flies forward with the original direction of rotation.

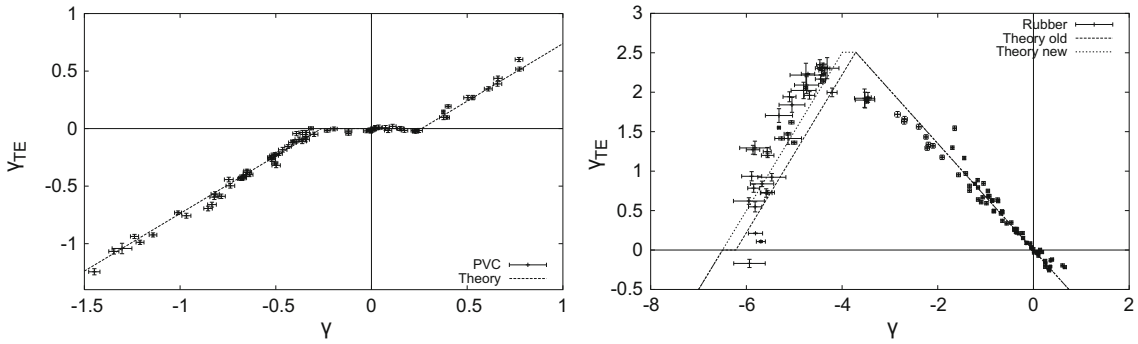

Fig. 7 Dimensionless tangential relative velocity, after versus before the impact, left PVC, right rubber

As a result, we may state that firstly for the rubber case the impact coefficient of restitution in normal direction depends much more on the velocities at collision than for stiff materials, that secondly we get a typical characteristic behavior in the sense of tangential reversibility, and that thirdly for soft materials like rubber we may have friction coefficients larger than one ($\mu > 1$). The theory describes this behavior very well, where especially for soft materials a correction according to Eq. (11) makes sense.

Figure 7 shows results of experiments with a PVC test body. The experiments are marked by crosses, the dotted line shows the theoretical result. For small tangential relative velocities before the impact, sticking occurs, and the rolling constraint between disk and ground is fulfilled after the impact. If the relative velocity is big enough, the body slides throughout the impact and has a reduced tangential relative velocity at the end of the impact. No tangential reversion occurs. In the area around zero tangential speed, we get sticking.

A similar diagram for a rubber body is shown in Fig. 7. For most of the impacts, the tangential relative velocity has changed during the impact: The bodies collide with a negative relative velocity and separate with a positive velocity. The inclination of the line through the origin is $-\varepsilon_N \varepsilon_T$. If ε_N is known from another simple experiment one can evaluate the coefficient of tangential reversibility from this plot. For this series of experiments, the parameters $\varepsilon_N = 0.75$ and $\varepsilon_T = 0.9$ were identified.

If the tangential relative velocity increases further, sliding occurs in the contact point during the impact. Then it is not possible to restore the elastic potential energy during the phase of expansion. For very high velocities, the rubber body slides during the whole impact, and the effect of tangential reversibility is not further visible.

In Fig. 7 two lines are plotted for comparing theory with experiment. What is called "Theory old" corresponds to the original theory of impacts with friction as presented in Glocker's dissertation [6]. What is called "Theory new" includes the extension as given by Beitelschmidt [3] (Eq. 11), which applies mainly for very soft material pairings. If we consider the contact point of two bodies, where Coulomb's friction applies, and that point of the contact zone, where the spring force resulting from the storage of impulse applies, we come out with two force laws in series. This gives a modification of the complementarities with respect to the friction cone, and thus a modification of the final results.

5 Examples

5.1 The central simple impact

In the following we shall apply the above impact models to the example of a central impact (Beitelschmidt [3]), giving already an impression of the complexity of impact dynamics. Going further to multiple impacts in multibody systems we must apply numerical methods. Therefore, it makes sense to study the structure of such impacts with the help of simple examples, which can be solved analytically.

We assume for the following that the initial relative velocities are always negative, $\dot{g}_{NA} < 0$, $\dot{g}_{TA} < 0$. This does not influence the generality, because for positive values we would get symmetrical results. We introduce, in addition to Eq. (30), the subsequent dimensionless quantities:

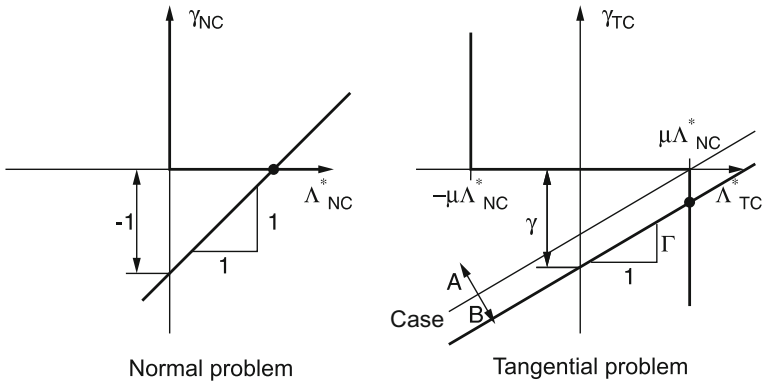

Fig. 8 Compression of the central simple impact

$$\Lambda^*_{NC} = \frac{G_{NN}}{-\dot{g}_{NA}}\Lambda_{NC}, \quad \Lambda^*_{TC} = \frac{G_{NN}}{-\dot{g}_{NA}}\Lambda_{TC} \quad \Lambda^*_{NE} = \frac{G_{NN}}{-\dot{g}_{NA}}\Lambda_{NE}, \quad \Lambda^*_{TE} = \frac{G_{NN}}{-\dot{g}_{NA}}\Lambda_{TE}, \quad \Gamma = \frac{G_{TT}}{G_{NN}}. \tag{31}$$

The reduction of the general equation (Chapter 2.1) for the compression phase of the central simple impact comes out with:

$$\gamma_{NC} \geq 0, \quad \Lambda^*_{NC} \geq 0, \quad \gamma_{NC}\Lambda^*_{NC} = 0 \qquad \text{with} \quad \gamma_{NC} = \Lambda^*_{NC} - 1, \tag{32}$$

$$\gamma_{TC} = \begin{cases} < 0 \text{ if } & \Lambda^*_{TC} = \mu\Lambda^*_{NC} \\ 0 \text{ if } & -\mu\Lambda^*_{NC} < \Lambda^*_{TC} < \mu\Lambda^*_{NC} \\ > 0 \text{ if } & \Lambda^*_{TC} = -\mu\Lambda^*_{NC} \end{cases} \qquad \text{with} \quad \gamma_{TC} = \Gamma\Lambda^*_{TC} - \gamma. \tag{33}$$

All equations represent straight lines in the appropriate velocity–impulse planes as depicted in Fig. 8, where the constraints of Eqs. (32) and (33) appear as the corresponding corner laws. The normal problem on the left-hand side of Fig. 8 possesses obviously the solution

$$\Lambda^*_{NC} = 1 \quad \text{and} \quad \gamma_{NC} = 0$$

defining the end of compression for the case under consideration. The tangential problem must have three solutions depending on the value of γ, either "sliding left" or "sliding right" or "stiction". For the above defined negative γ we have only two cases:

$$\begin{aligned} &\text{Case A: } \gamma > -\mu\Gamma \ \gamma_{TC} = 0 \qquad \Lambda^*_{TC} = \tfrac{\gamma}{\Gamma} \text{ stick} \\ &\text{Case B: } \gamma < -\mu\Gamma \ \gamma_{TC} = \gamma + \mu\Gamma \ \Lambda^*_{TC} = \mu \text{ slip.} \end{aligned} \tag{34}$$

The expansion phase even of the central simple impact is more complicated due the stored impulses, which must be taken into consideration. A specialization of the general equations to our case gives for the normal problem the relations:

$$\gamma_{NE} = \Lambda^*_{NE} + \gamma_{NC}, \tag{35}$$

$$\gamma_{NE} \geq 0, \quad (\Lambda^*_{NE} - \varepsilon_N\Lambda^*_{NC}) \geq 0, \quad \gamma_{NE}(\Lambda^*_{NE} - \varepsilon_N\Lambda^*_{NC}) = 0. \tag{36}$$

The situation is depicted in Fig. 9, left-hand side, which is self-explaining. The solution point for the end of the expansion has the coordinates:

$$\gamma_{NE} = \varepsilon_N \quad \text{und} \quad \Lambda^*_{NE} = \varepsilon_N. \tag{37}$$

The tangential problem is first characterized be the double corner of Fig. 2 and the relevant equations. This double corner can again been detected in the right-hand diagram of Fig. 9. Its vertical limits are clear, the horizontal limit results from Eq. (11) and has the following value:

$$\gamma_{TE0} = \varepsilon_N\varepsilon_T\Gamma\Lambda^*_{TC}. \tag{38}$$

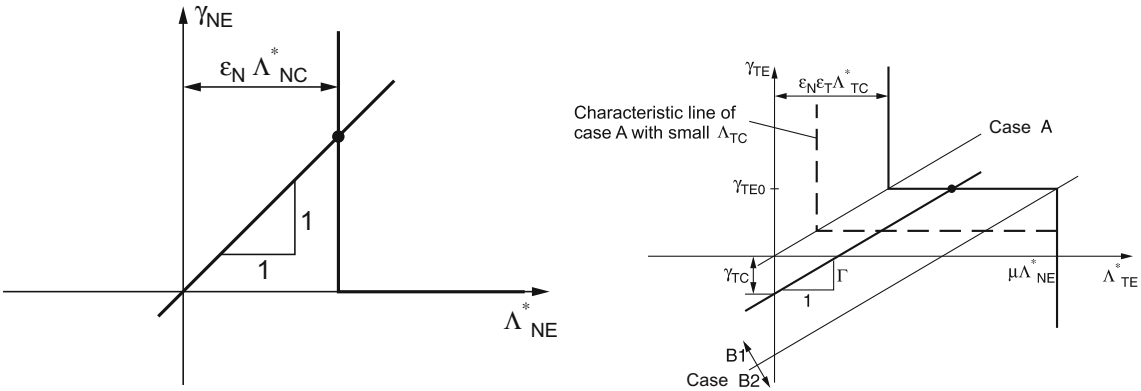

Fig. 9 Expansion for the central simple impact

To find a solution for that case we firstly must consider the impulse budget,

$$\gamma_{TE} = \Gamma \Lambda^*_{TE} + \gamma_{TC}, \tag{39}$$

which is a straight line in the $\gamma_{TE} - \Lambda^*_{TE}$ - plane, and we secondly must consider the two tangential solution cases at the end of compression according to Eq. (34):

- **Case A**: At the end of compression we have stiction with $\gamma_{TC} = 0$ and with a tangential impulse $\Lambda^*_{TC} = -\gamma/\Gamma$. From this we get a correction velocity of $\gamma_{TEO} = -\varepsilon_N \varepsilon_T \gamma$. Therefore, the impulse equation cuts the double corner characteristic exactly in the left corner. This means physically that during compression a tangential impulse will be stored, which due to stiction can be regained more or less completely.
- **Case B**: At the end of compression, we have sliding with $\Lambda^*_{TC} = \mu$ for the tangential impulse. The horizontal line of the double corner is then located at

$$\gamma_{TE0} = \varepsilon_N \varepsilon_T \mu \Gamma \tag{40}$$

and thus does not depend on the initial conditions. If we shift the impulse line in a parallel way until it meets the right corner point of the impact characteristic, we come out with $\gamma_{TC} = \Gamma \mu \varepsilon_N (\varepsilon_T - 1)$. If γ_{TC} remains above this line, we get a case **B1** with the following relative tangential velocity and the tangential expansion impulse:

$$\gamma_{TE} = \varepsilon_N \varepsilon_T \gamma, \qquad \Lambda^*_{TE} = \mu(\varepsilon_N \varepsilon_T - 1) - \frac{\gamma}{\Gamma}. \tag{41}$$

This case can be physically generated by a combination of sliding during compression and stiction during expansion, where the stored impulse is again released. If γ_{TC} remains under the above defined line, we get a case **B2** with the following values for velocity and impulse:

$$\Lambda^*_{TE} = \mu \varepsilon_N, \qquad \gamma_{TE} = \mu \Gamma (1 + \varepsilon_N) + \gamma. \tag{42}$$

The impulse line always cuts the right vertical characteristic of the impact law, which means sliding during the complete impact. The results of the tangential problem for the central simple impact are summarized in Table 1.

The theory has been simulated for many data sets and in addition verified by measurements. To give only one example we consider the following dataset (Table 2):

The results are depicted in Fig. 10, where the tangential relative velocities after and before an impact are given. The kinks of the curves indicate the above discussed areas **A**, **B1**, and **B2**. If $\varepsilon_T > 0$, we get in the neighborhood of $\gamma = 0$ a reversal of the relative tangential velocity, which physically corresponds to a weak impact with a small relative velocity. If the relative tangential velocity is very large, we have more or less only sliding during the whole impact, and no reversal will be possible. With corresponding measurements the coefficient of restitution in tangential direction ε_T can be evaluated directly from the slope of the curves around the origin. It should be noted that the theoretical lines as shown in Fig. 7 are evaluated applying the calculations of Fig. 10.

Table 1 The tangential problem of the central simple impact

	Compression				
Value	Case A	Limit	Case B		
	$0 > \gamma > -\mu\Gamma$	$\gamma = -\mu\Gamma$	$\gamma < -\mu\Gamma$		
γ_{TC}	0	0	$\gamma + \mu\Gamma$		
Λ^*_{TC}	$-\frac{\gamma}{\Gamma}$	μ	μ		
	Expansion, $\gamma_{lim} = -\mu\Gamma(1 + \varepsilon_N - \varepsilon_N\varepsilon_T)$				
			Case B1	Limit	Case B2
			$\gamma > \gamma_{lim}$	$\gamma = \gamma_{lim}$	$\gamma < \gamma_{lim}$
γ_{TE}	$-\varepsilon_N\varepsilon_T\gamma$	$\mu\varepsilon_N\varepsilon_T\Gamma$	$\mu\varepsilon_N\varepsilon_T\Gamma$	$\mu\varepsilon_N\varepsilon_T\Gamma$	$\mu\Gamma(1+\varepsilon_N)+\gamma$
Λ^*_{TE}	$-\varepsilon_N\varepsilon_T\frac{\gamma}{\Gamma}$	$\varepsilon_N\varepsilon_T\mu$	$\mu(\varepsilon_N\varepsilon_T - 1) - \frac{\gamma}{\Gamma}$	$\mu\varepsilon_N$	$\mu\varepsilon_N$
	Overall impact				
Λ^*_T	$-(1+\varepsilon_N\varepsilon_T)\frac{\gamma}{\Gamma}$	$(1+\varepsilon_N\varepsilon_T)\mu$	$\mu\varepsilon_N\varepsilon_T - \frac{\gamma}{\Gamma}$	$\mu(\varepsilon_N+1)$	$\mu(\varepsilon_N+1)$

Table 2 Simulated data sets

Set	Γ	μ	ε_N	ε_T	Description
1	2.5	0.5	0.8	0.0	No tang. reversibility
2	2.5	0.5	0.8	0.4	Small tang. reversibility (like steel)
3	2.5	0.5	0.8	0.8	$\varepsilon_N = \varepsilon_T$ (like rubber)
4	2.5	0.5	1	1	Energy conservation

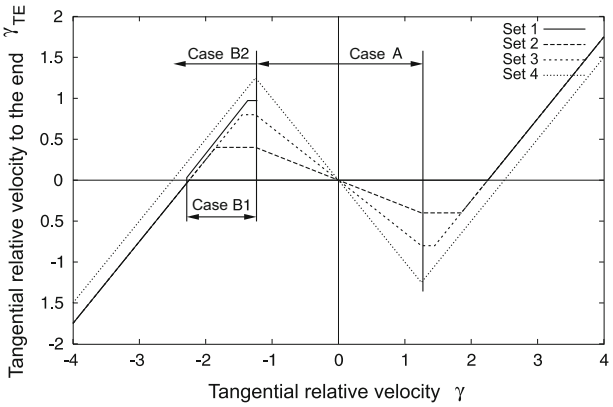

Fig. 10 Relative tangential velocities for the central simple impact

5.2 Vibration conveyor

Vibratory feeders are used in automatic assembly to feed small parts. They are capable to store, transport, orient and isolate the parts. An oscillating track with frequencies up to 100 Hz excites the transportation process, which is mainly based on impact and friction phenomena between the parts and the track. Vibratory feeders are applied for a wide variety of parts and for lots of different tasks. In the majority of cases, the parts are available as a sort of bulk material that is stored in a container. The transportation process, starting in this reservoir, is often combined with orienting devices that orient parts, or select only these parts having already the right orientation (Fig. 11 shows an example of a vibratory bowl feeder with an orienting device). Each kind of parts, with its special geometry and mechanical properties, requires an individual adaption of the feeder. This individual tuning comprises the development of suitable track and orienting device geometries and the adjustment of the excitation parameters frequency and amplitude. Due to the complex mechanics of the feeding process, this design is usually done by trial and error without any theoretical background. A complete dynamical model of the transportation process allows a theoretical investigation and consequently an improvement of the feeder properties [20,21].

Friction and impact phenomena between the parts and the track are the most important mechanical properties of transportation processes. Consequently, the required dynamical model has to deal with unilateral constraints, dry friction and multiple impacts. The mechanical model of the vibratory feeder can be split in two parts: the transportation process and the base device. The dissertation [20] focuses on modeling and simulation of the

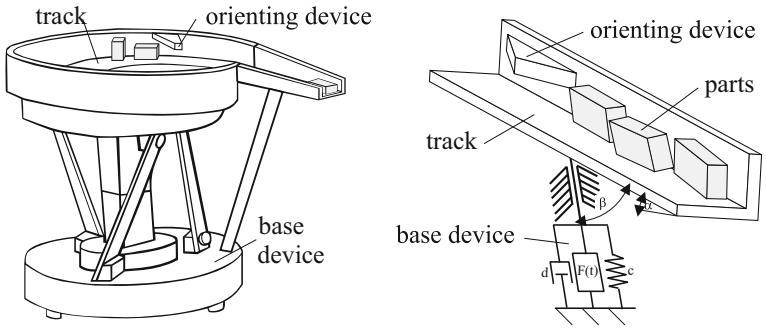

Fig. 11 Vibratory bowl feeder and mechanical model

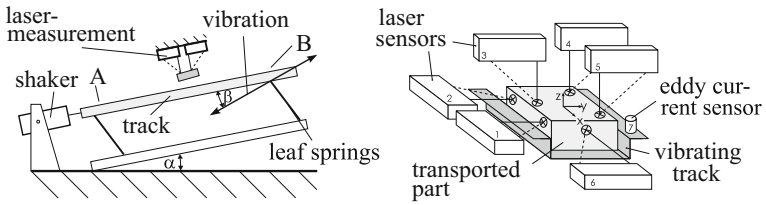

Fig. 12 Test setup and part measurement

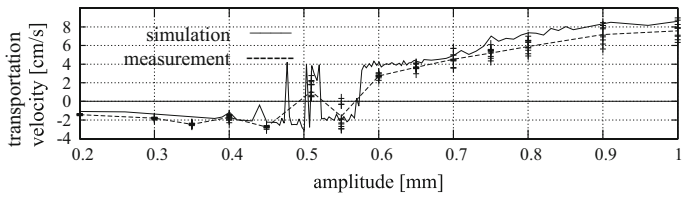

Fig. 13 Simulation and measurement of the average transportation rate

transportation process. The modeling of the base device can be done with well-known standard techniques for multibody systems.

For the verification of the developed model of the transportation process, an experimental vibratory feeder was built, allowing different measurements concerning the impact model and the average transportation rates. Figure 12 shows the principle of the device. The track, fixed on leaf springs, is excited with an electromagnetic shaker with a frequency about 50 Hz. The eigenfrequency of the system is at 52 Hz. The resulting vibration amplitude reaches a maximum value of about 2 mm. The track has an inclination angle $\alpha = 3°$, the angle between the track and the direction of the vibration is $\beta = 15°$. For the accurate contactless measurement of the motion of the transported part six laser distance sensors were applied. For the vibration measurement of the track, an eddy current sensor is used.

For a comparison of the theory and the measurements the averaged transportation rate has been considered. Figure 13 gives a result, which before the background of the complexity of the problem looks good. An interesting finding is the fact that the averaged transportation velocity does not depend very much on the number of parts and also not on the type of modeling, plane or spatial [20]. Therefore, the design of vibration conveyors can be performed considering one part only. For the layout of orienting devices, we need of course a spatial theory.

6 Conclusions

We consider impacts with friction in multibody systems. A classical approach for modeling applies the complementarity idea for contacts and comes out with the necessary solution of linear or nonlinear complementarity problems. The second and more modern approach uses measure differential equations in combination with the concept of proximal functions to describe the contact and impact behavior. Both methods have to be treated numerically, where the second method offers a couple of advantages with respect to numerics. After a

careful discussion of the energy losses of frictional impacts, we present measurements with a very successful comparison of theory and experimental results.

Impacts with friction must be analyzed with the help of computers. An exception is the simple central impact, which turns out to be not so simple as seen from a first glance. This case has been considered analytically. As a representative from industry we give some typical results for a vibration conveyor. It may be seen as pars pro toto. Many industrial problems with impacts and friction have been solved in the meantime [15,18].

References

1. Alart, P., Curnier, A.: A mixed formulation for frictional contact problems prone to Newton like solution methods. Comput. Methods Appl. Mech. Eng. **92**, 353–375 (1991)
2. Beitelschmidt, F., Pfeiffer, M.: Experimental investigation of impacts with friction. In: Pfeiffer, F., Glocker, Ch. (eds.) IUTAM Symposium on Unilateral Multibody Contacts, pp. 71–80. Kluwer, Boston (1999)
3. Beitelschmidt, M.: Reibstösse in Mehrkörpersystemen. Fortschritt-Berichte VDI, Reihe 11, Nr. 275. VDI-Verlag Düsseldorf (1999)
4. Foerg, M.: Mehrkörpersysteme mit mengenwertigen Kraftgesetzen—Theorie und Numerik. Fortschritt-Berichte VDI, Reihe 20, Nr. 411. VDI-Verlag Düsseldorf (2007)
5. Foerg, M., Geier, T., Neumann, L., Ulbrich, H.: r-Factor strategies for the augmented Lagrangian approach in multi-body contact mechanics. In: II European Conference on Computational Mechanics, Lisboa (2006)
6. Glocker, C.: Dynamik von Starrkörpersystemen mit Reibung und Stössen. Fortschritt-Berichte VDI, Reihe 18, Nr. 182, VDI-Verlag Düsseldorf (1995)
7. Glocker, C.: Set-Valued Force Laws—Dynamics of Non-Smooth Systems. Springer, Berlin (2001)
8. Glocker, C.: Energetic consistency conditions for standard impacts, part I: Newton-type inequality impact laws and Kane's example. Multibody Syst. Dyn. **29**(1), 77–117 (2013)
9. Glocker, C.: Energetic consistency conditions for standard impacts, part ii: Poisson-type inequality impact laws. Multibody Syst. Dyn. **32**(4), 445–509 (2014)
10. Leine, R.I., Nijmeijer, H.: Dynamics and Bifurcations of Non-Smooth Mechanical Systems. Springer, Berlin (2004)
11. Moreau, J., Panagiotopoulos, P.: Unilateral Contact and Dry Friction in Finite Freedom Dynamics, volume 302. International Center of Mechanical Sciences (CISM), Courses and Lectures. Springer, Wien (1988)
12. Panagiotopoulos, P.D.: Hemivariational Inequalities. Springer, Berlin (1993)
13. Papastavridis, J.G.: Analytical Mechanics. Oxford University Press, Oxford (2002)
14. Pfeiffer, F.: Applications of unilateral multibody dynamics. Philos. Trans. R. Soc. Lond. A **359**, 2609–2628 (2001)
15. Pfeiffer, F.: Mechanical System Dynamics. Springer, Heidelberg (2008)
16. Pfeiffer, F., Glocker, C.: Multibody Dynamics with Unilateral Contacts. Wiley, New York (1996). Within the Wiley Series of Nonlinear Science (Ed. Ali Nayfeh). (1996)
17. Rockafeller, R.T.: Convex Analysis. Princeton University Press, Princeton (1970)
18. Schindler, T.: Spatial Dynamics of Pushbelt CVTs. Fortschrittberichte VDI, Reihe 12, vol. 730. VDI-Verlag Düsseldorf (2010)
19. Schindler, T., Nguyen, B., Trinkle, J.: Understanding the difference between prox and complementarity formulations for simulation of systems with contact. In: 2011 International Conference on Intelligent Robots and Systems, San Francisco, CA, pp. 1433–1438 (2011)
20. Wolfsteiner, P.: Dynamik von Vibrationsförderern. Fortschrittberichte VDI, Reihe 2, Nr. 511. VDI-Verlag Düsseldorf (1999)
21. Wolfsteiner, P., Pfeiffer, F.: The parts transportation in a vibratory feeder. In: IUTAM Symposium on Unilateral Multibody Dynamics, München (1998)